PJET, Vol. 4, No. 2, August 2026: 1-28

Poly Journal of Engineering and Technology

journal homepage: https://journals.bdu.edu.et/index.php/PJET/index

ORGINAL ARTICLE

Geographical Origin Determination of Ethiopian Teff Using Multi-Channel Capsule Networks

Habtamu Ayalew Aycheh[1], Dires Workie Sefineh[1*], Fentahun Yirsaw Tiruneh[1], Afework Abiye Jenber[2], Abrham Debasu Mengistu[1]

[1] Faculty of Computing, Bahir Dar Institute of Technology, Bahir Dar University, Bahir Dar, Ethiopia

[2] Faculty of Mechanical and Industrial Engineering, Bahir Dar Institute of Technology, Bahir Dar University, Bahir Dar, Ethiopia

ABSTRACT

Agriculture plays a vital role in food security and economic development in developing countries like Ethiopia. Precisely identifying the geographical origin of agricultural products like Teff is challenging because different varieties may have the same size, color, and shape. This study applies computer vision with multi-channel capsule network algorithm architecture to identify the geographical origin of Ethiopian Teff. The proposed approach overcomes the traditional CNN's challenges related to viewpoint variation, overfitting, and spatial variation for red and mixed varieties of Teff. The images of Teff were collected from various locations in the Amhara region of Ethiopia. Image preprocessing techniques used in this work include median, Gaussian, and non-local means filtering to enhance the image quality. Content-aware resizing was applied to resize the images, and Contrast Limited Adaptive Histogram Equalization (CLAHE) was used to enhance image contrast. For image segmentation, we used multi-Otsu thresholding, region-based segmentation, watershed segmentation, and U-Net to identify the regions of interest in the Teff images. Subsequently, we extracted features from the segmented images using the BRISK and HOG methods. Once the feature vectors were obtained, we developed a model using Capsule Networks to determine the geographical origin of Ethiopian Teff. A total of 11 distinct experiments took place and achieved notable results in three different approaches. The first approach, using the BRISK feature extraction method, combined Multi-Otsu thresholding, region-based segmentation, watershed segmentation, and comprehensive noise removal, achieved the highest accuracy of 84%. In the second approach, when combining region-based segmentation with that of median and Gaussian filtering, along with BRISK feature extraction, achieved an accuracy of 80%. The third approach, using Histogram of Oriented Gradients (HOG) feature extraction, combined with Multi-Otsu thresholding, region-based segmentation, watershed segmentation, and comprehensive noise removal, achieved a good accuracy of 92.5%. These findings demonstrate that our proposed model can accurately identify the geographical origin of Ethiopian Teff with a test accuracy of 92.5% performance.

Keywords: Multi-Channel Capsule Network; Deep Learning; Teff classification; Image Processing, Computer vision; Geographical Origin Determination

DOI: https://doi.org/10.20372/pjet.v4i2.3700

Corresponding Author: **Dires Workie Sefineh**

Email: Corresponding author: **Corresponding author:* abushuworkie@gmail.com

1. Introduction

Agriculture is the main source of Ethiopian economy that covers overs 85% of the population and contributing to food security and exports [1]. Teff holds the particular cultural and economic significance and the primary grain of preparing injera. It is the smallest grain in size accross the world approximately 1 mm. It is primarily cultivated in the Amhara and Oromia regions, and in smaller quantities in Tigray and SNNP [2] regions. Teff can be categorized into three types including white, red, and mixed. Despite its economic and other relevance, the accurate geographical origin determination of Teff remains a major problem and it is unexplored. The white teff commands premium prices due to its restricted growing conditions and consumer preference. White Teff from specific high-altitude regions commands 30 to 50% higher prices than mixed varieties from lower altitudes [3]. This price variation creates a strong economic incentive for misrepresentation. The traders as well as producers may falsely label lower-value of Teff as originating from relevant regions to receive higher market prices. This human attitude may harm market integrity, defraud consumers, and harm legitimate producers. In addition to this problem, Teff varieties from different regions have different morphological differences in size, shape, and also in color. These morphological differences are not easily visible and identified by the human eye. Even experienced agronomists at the Adet Agricultural Research Center acknowledge that visual identification is unreliable and prone to error [4]. This visual similarity can lead to fraud in Teff trading, where mislabeling can be difficult to detect without laboratory analysis automatic tools. Recent advances in artificial intelligence, such as deep learning and computer vision approaches have great performance in agricultural applications, including crop identification, quality assessment, and classification [5-7]. These studies have explored the deep learning and computer vision techniques for different tasks like fruit grading [8], maize seed classification [9], coffee bean classification [10], and tomato classification [11]. However, applying these techniques to Teff origin determination have its own challenges. This is because the Teff grain size and subtle inter-regional morphological variations [12] are significantly different from other agricultural products. Existing machine learning approaches for Teff origin determination have two main critical limitations. The first limitation is a limited variety and region coverage. The only previous study in [13] focused exclusively on white Teff from four regions. This study excluded red and mixed varieties that have vital market segments and failing to represent the full complexity of the Teff supply chain. The second is the fundamental CNN approach limitations. While CNNs have been widely used in agricultural classification, they suffer from inherent limitations that are particularly problematic for Teff grain classification [14, 15]. In this study, we proposed a multi-channel capsule network with computer vision for determining the geographical origin of Ethiopian Teff. This approach addresses the spatial invariance, viewpoint variance, and limited variety or region coverage limitations of previous CNN-based approaches.

2. Related Works

Previous study [16] developed a tomato classification model with a total dataset of 5,266 images from 7 different tomato species. The images were primarily resized into 150x150 pixel sizes. In this paper the Deep CNN approach was used in order to extract features and perform classification by incorporating Max Pooling layers. The dataset was divided into training 70% and validation 30% subsets. The training accuracy achieved a performance of 99.99%, and the validation accuracy achieved a performance of 93%. However, it is important to note that training CNNs typically requires a typical amount of annotated data. In addition to that image reconstruction can pose challenges when using max pooling. As a result, there is still room for improvement in tomato classification methods. Furthermore, Teff presents additional challenges compared to tomatoes due to its significantly smaller size. Thus, the development of an improved approach is necessary to accurately identify the geographical origin of Teff.

The study by [17] developed the distinction between peaberry and normal beans model was investigated. A total of 3,338 datasets images was used. The images then resized into 32×32 pixel size, 64×64 pixel size, 128×128 pixel size, and 256×256 pixel size. The researchers used CNN and Support Vector Machines (SVM) algorithm for classification purpose. The experimental results shows that the CNN have higher performance than the SVM in determining the peaberry beans. The image processing techniques were used to grade the raw quality of Ethiopian coffee in the study [18]. In this study a total of 10,000 coffee bean images were used. They additionally used yhe thresholds for segmentation and a Gaussian blur filter to remove noise. They also used an 80% dataset for training and a 20% dataset for testing. The ANN, SVM, and KNN techniques are used for classification. ANN classifier showed the highest accuracy of 89.64% than the others. However, they did not use alternative segmentation techniques, nor did they consider the algorithms of CNN and CapsNets.

In the paper [19], the authors identify the banana ripeness stage using a deep learning approach. The banana ripeness is divided into four different stages. A total of 273 images dataset were used, and then splitted 80% of the data in each stage used for training and 20% of the data used for testing. They used a CNN for classification, but it requires a huge number of images for training to achieve better classification results. Based on this, they augmented the original images, then trained and tested both the original and augmented images. The CNN model was trained with an overall validation accuracy of 96.14% compared with VGGNet16 and ResNet50. But unlike CNN, capsule networks don't need a huge number of images. In a recent study by [20]. The researchers explored the recognition of Shiro flour variety using a combination of CNN and Gray-Level Co-occurrence Matrix (GLCM) features. A dataset of 6,000 images for this investigation. Different techniques like the GLCM, CNN (for automatic feature extraction), and the combination of CNN and GLCM (traditional feature extraction) are used. The researchers used the CNN, SVM, and KNN algorithms in order to classify the Shiro flour variety. The results showed that the combined feature vectors of CNN and GLCM used with the KNN classifier achieved the best accuracy of 99.9% performance. However, the authors note that while the CNN and KNN algorithms performed well, they are traditional approaches compared to the more recent CapsNets. This may offer advantages in capturing the unique structural characteristics of the Shiro flour variety.

In the study conducted by [21] Teff geographical identification model was developed. The researchers used a total of 3,088 Teff images and implemented on the MATLAB experimental tool. They also applied the preprocessing techniques. These preprocessing techniques like Brightness Preserving Bi Histogram Equalization (BBHE), median and Gaussian filters for noise removal, and combined thresholding with Mask R-CNN for image segmentation. The researchers used the (CNN) and the BRISK algorithms for feature extraction. The different classification algorithms are evaluated, including Multi-class Support Vector Machine (SVM), CNN, and a combined SVM-CNN approach, with Principal Component Analysis (PCA) also applied. The proposed Multi-class SVM classifier achieved a training accuracy of 97.66% and a testing accuracy of 92.02% in identifying the geographical origin of Teff. However, the study noted limitations such as spatial invariance, data structure understanding, and viewpoint variance issues in CNN, which can increase the misclassification error, as well as the potential for overfitting and training on noisy image data. Additionally, CNN-based models can be easily fooled by carefully constructed noise in the input images, and the study focused only on white Teff from four geographical areas, which may limit the generalization to other Teff varieties and regions. When the literature review is examined, it is observed that CNN-based algorithms are frequently used for the classification of different agricultural products. However, the natural complexity of different agricultural product images still limits the performance of many CNN models. In our study, we develop a multi-channel capsule network with computer vision to determine the geographical origin of Teff to fix these limitations.

3. Materials and Methods

The proposed model incorporates three components, including image preprocessing, feature extraction, and classification. In image preprocessing, a series of steps, such as resizing using content-aware, noise removal using a combination of median, Gaussian, and non-local means denoising techniques, are applied. Histogram equalization techniques were used to improve the contrast of RGB images by effectively spreading out the most frequent intensity values. After the image is converted into grayscale, the Contrast Limited Adaptive Histogram Equalization (CLAHE) was used before applying image segmentation. After getting the CLAHE image, the segmentation phase took place. The image segmentation techniques, such as multi Otsu's thresholding, region-based and watershed segmentations, as well as deep learning-based image segmentation U-Net, were used for this study. Then after, from the segmented images, feature extraction was performed using HOG (Histogram of Oriented Gradients) and Binary Robust Invariant Scalable Key Points (BRISK) vector used to enhance the feature extraction technique for Teff feature extraction. Finally, the extracted feature vector is fed to CapsNets for developing the model that helps to determine Ethiopian Teff based on their geographical origins. The high-level model architecture is depicted in Figure 1.

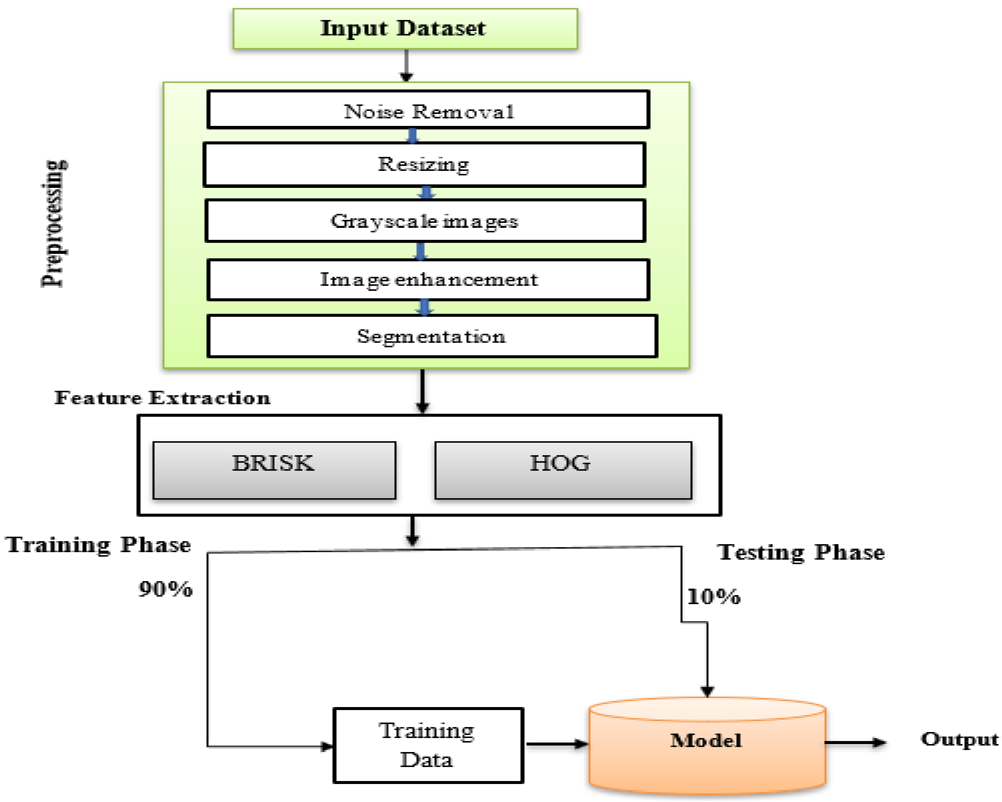

Figure 1: The proposed model architecture

3.1. Image Preprocessing

The image is often affected by background distortions like noise, illumination variations, and shadows. These distortions can limit the critical information. To address these challenges, we applied preprocessing to reduce noise and improve image contrast while preserving relevant image information. In this proposed study, the image processing techniques, including image resizing, histogram equalization (HE), noise reduction, segmentation, image scaling, and contrast enhancement, were used on Teff images.

3.1.1. Noise removal

In this study, we captured the Teff images on white paper. This helps to reduce the noise. Salt-and-pepper noise (dust) and other noise types that happen during image acquisition of the image. To remove such noise, we used median, Gaussian, and non-local means denoising filter techniques that increased the image quality, according to [22, 23]. To achieve effective noise removal while preserving important details, we used a combination of techniques. We started by applying a median filter to remove impulse noise, such as salt-and-pepper noise, which might be present in Teff grain images. As depicted in Figure 2, the median filter replaces each pixel value with the median value of its neighborhood, effectively reducing the impact of outliers.

Figure 2: Noise removal using median filtering

As depicted in Figure 3 we applied a Gaussian filter to reduce Gaussian noise, which is a type of random noise commonly found in images. The Gaussian filter convolves the image with a Gaussian Kernel, smoothing out the image and reducing high-frequency noise while preserving the overall structure. The Gaussian filter's blurring effect complements the edge-preserving properties of the median filter.

Figure 3: Noise removal using Gaussian filtering

Lastly, we applied non-local means denoising to further reduce both random and structured noise. This technique compares patches within the image to estimate the true pixel values, effectively reducing noise while preserving textures and details.24]. Applying this after the median and Gaussian filters can help remove any remaining noise while preserving important details. The denoised teff image with non-local means is represented in

Figure 4.

Figure 4: Noise removal using non-local means denoising

3.1.2. Resizing(resampling) of Image

Rather than a traditional resizing method, a content-aware seam carving, introduced by [25] was used to resize an image. This is a especially important when maintaining the aspect ratio is crucial. In this technique, a seam refers to an 8-connected path of pixels in the horizontal or vertical direction, with one pixel per row [26]. This helps for our proposed model to preserve the integrity of important objects or structures in the image. This minimizes distortions or information loss compared to traditional resizing methods.

3.1.3. Conversion to Grayscale

When we train our proposed model primarily it receives input images in the RGB color space. In order to simplify the computational requirements of the proposed model, the normal RGB image is converted into a grayscale image format. This conversion stage is important because of grayscale images only contain intensity information. This makes easier to process compared to RGB images [27]. Considering our proposed input dataset diverse colors, using grayscale can ensure consistent prediction methodologies. The conversion from RGB to grayscale is a well-established technique that reduces the dimensionality of the input data by preserving the necessary image information. Figure 5 illustrates representative Teff images before and after grayscale conversion.

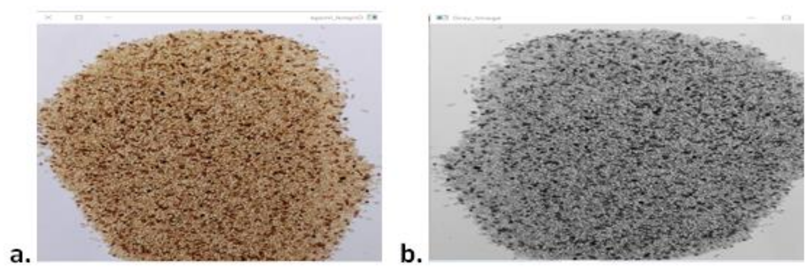

Figure 5: Grayscale conversion of Teff grain images. (a) Original RGB images; (b) corresponding grayscale images

3.1.4. Histogram Equalization

In this proposed study, we used the CLAHE technique that applies contrast limiting to each neighborhood to derive a transformation function [28]. The CLAHE is good for images with speckle noise, low-contrast regions, and resolvable details. It also prevents over-amplification of noise. The CLAHE computes multiple histograms each for a distinct image region, and uses them to redistribute lightness values. This can improve the local contrast, edge definitions, texture features, and overall image structure. Figure 6 shows representative Teff images before and after CLAHE application.

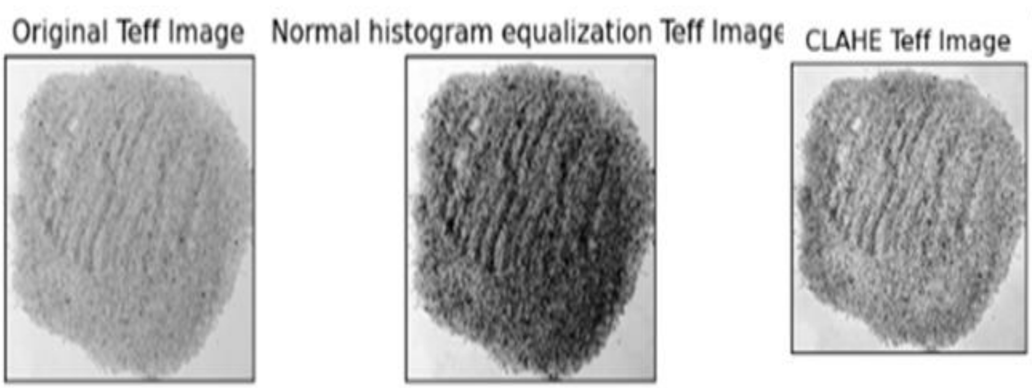

a) b) c)

Figure 6: CLAHE enhancement on Teff grain images. (a) Original grayscale Teff images; (b) corresponding CLAHE-enhanced images; (c) histogram comparison showing intensity redistribution and contrast stretching

3.1.5. Image Segmentations

Image segmentation is the process of dividing a digital image into a set of pixels or multiple regions [29]. In the context of Capsule Networks, segmentation is essential for minimizing computational time and extracting representative features as identifiers. The primary objective of image segmentation is to simplify the image for improved analysis. In this study, we used a combination of Otsu's thresholding, region-based segmentation, watershed segmentation, and U-Net segmentation in deep learning to isolate relevant features from the rest. Otsu's thresholding is a measure of thresholding that reduces the variation within two sets of pixels (background and foreground) by creating a histogram and finding an optimal threshold [30]. Multi-Otsu thresholding separates pixels in an input image into several different classes based on the intensity of gray levels. In the case of Teff grain images, where multiple intensity levels or classes can exist within the grains, multi-Otsu thresholding is a useful technique. This technique automatically determines optimal threshold values based on the image's intensity distribution, aiding in the division of the image into multiple regions or classes. Figure 7 shows representative Teff images before and after Multi-Otsu thresholding segmentation.

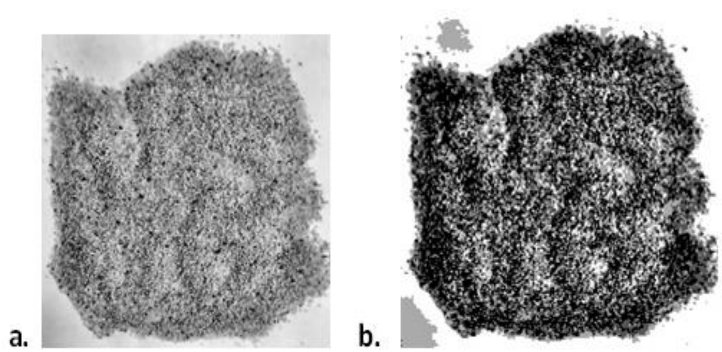

Figure 7: Multi-Otsu thresholding segmentation on Teff grain images. (a) Original grayscale Teff images; (b) Multi-Otsu thresholding results showing multi-class segmentation

Once the threshold values are obtained from multi-Otsu thresholding, we used region-based segmentation algorithms to further segment the image based on criteria such as texture, color, or intensity similarity. Region-based segmentation involves grouping pixels or regions with similar attributes and is commonly used to identify and separate objects or regions with similar characteristics in an image [31]. This approach is more resistant to noise and is particularly useful when it is straightforward to define similarity criteria for the desired segmentation task. Figure 8 illustrates representative Teff images before and after region-based segmentation.

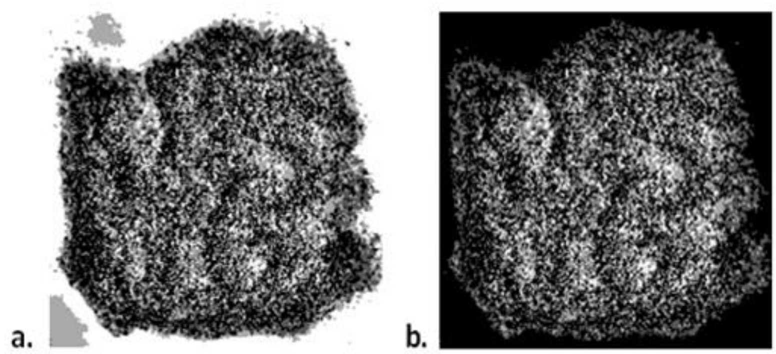

Figure 8: Region-based segmentation on Teff grain images. (a) Original grayscale Teff images; (b) region-based segmentation results showing coherent segmented regions

Finally, we apply watershed image segmentation to separate connected regions or fine details within the segmented regions obtained from the region-based segmentation. It helps in refining the segmentation by considering the gradient or edge information within the image. The watershed algorithm then simulates flooding the surface, starting from markers or seed points, and determines the boundaries between regions based on the flooding process [32]. Figure 9 illustrates representative Teff images before and after watershed segmentation.

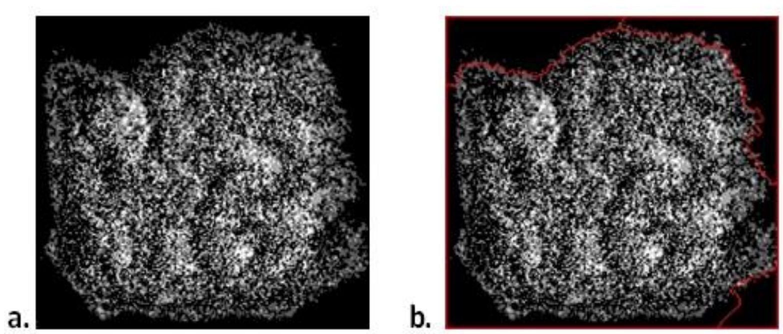

Figure 9: Watershed segmentation on Teff grain images. (a) Original grayscale Teff images; (b) watershed segmentation results showing separated grain regions

U-Net segmentation: U-Net segmentation is an enhanced, deep-learning-based convolutional neural network. It has the same encoder and decoder. An encoder is used to extract features, unlike fully adaptive networks that sample features using cross-connections. Cross-connections in U-Net are designed to solve the problem of data loss [33]. U-net are the ability to create very detailed segmentation maps. Figure 10 illustrates representative Teff images before and after U-Net segmentation, demonstrating the network's ability to produce detailed segmentation maps

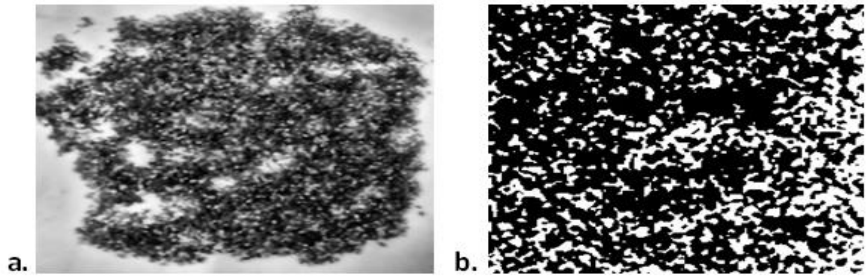

Figure 10: Images before (a) and after (b) using U-Net segmentation

3.2. Feature extractions

Following to the image segmentation phase, we followed the feature extraction. This feature extraction stage converts raw pixel data from segmented Teff images into a vector feature representation. Then after these extracted feature vectors are used as the input for next classification stage. This enables the model to learn effectively discriminate among Teff varieties from different geographical origins.

Histogram of Oriented Gradients (HOG): This feature extractor works by counting the frequencies of oriented gradients within localized parts of an image. HOG is a strong feature extractor because of its capability to capture the orientation and magnitude of gradients. This is particularly prominent at corners and edges where intensity changes occur. These edges help define the shape of an object [34]. By analyzing the distribution of gradients, HOG can effectively determine the appearance and shape of an object within an image. The figure in Figure 11 are the sample Teff images after Histogram of Oriented Gradients feature extraction.

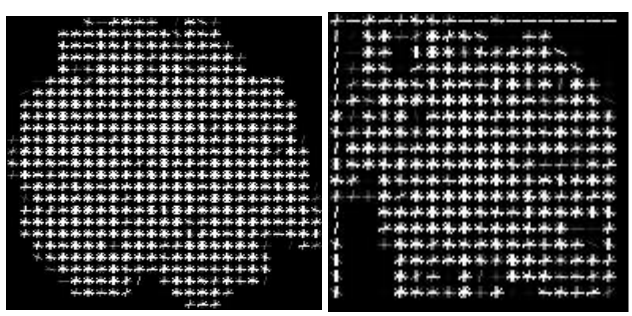

Figure 11: HOG feature extraction results on Teff grain samples

Binary Robust Invariant Scale Key Points (BRISK): BRISK is a local feature detection and description algorithm that achieves robust performance against image transformations, particularly rotation and scale variations [35]. It constructs a feature descriptor of the local image using the grayscale relationship of random points pairwise in the neighborhood of the image and obtains the binary feature descriptor. It is used for small objects. BRISK descriptors can be advantageous for applications with limited memory or computational resources, as it allows for efficient storage and comparison of the feature descriptors [36]. Figure 12 are the sample Teff images after the Binary Robust Invariant Scale Key Points feature extraction

a) b) c)

Figure 12: BRISK feature extraction visualization on representative Teff grain samples. (a) Original grayscale Teff images; (b) detected BRISK key points with scale (circle radius) and orientation (line direction); (c) binary descriptor sampling pattern around key

3.3. Classification

The Multi-channel capsule network is a recent deep learning architecture that overcomes the limitations of traditional CNNs [37]. It is a carrier containing a group of organized neurons, each representing various properties of an entity in the image, including position, size, direction, deformation, speed, hue, and texture. It accepts input as a vector and consists of a Convolutional layer, a Primary Capsule layer, a DigitCaps layer, and an encoder-decoder. A capsule's activity vector represents the probability of the entity's existence, and its orientation represents its instantiation parameters. Our proposed Multi-Channel Capsule Network based model employs a three-channel-based architecture designed to capture complementary feature hierarchies at different scales. The architecture comprises four main components, including a Convolutional Layer, Primary Capsule Layer (three parallel channels), Digit Capsule Layer, and Classification Layer. Figure 13 illustrates the complete architectural diagram.

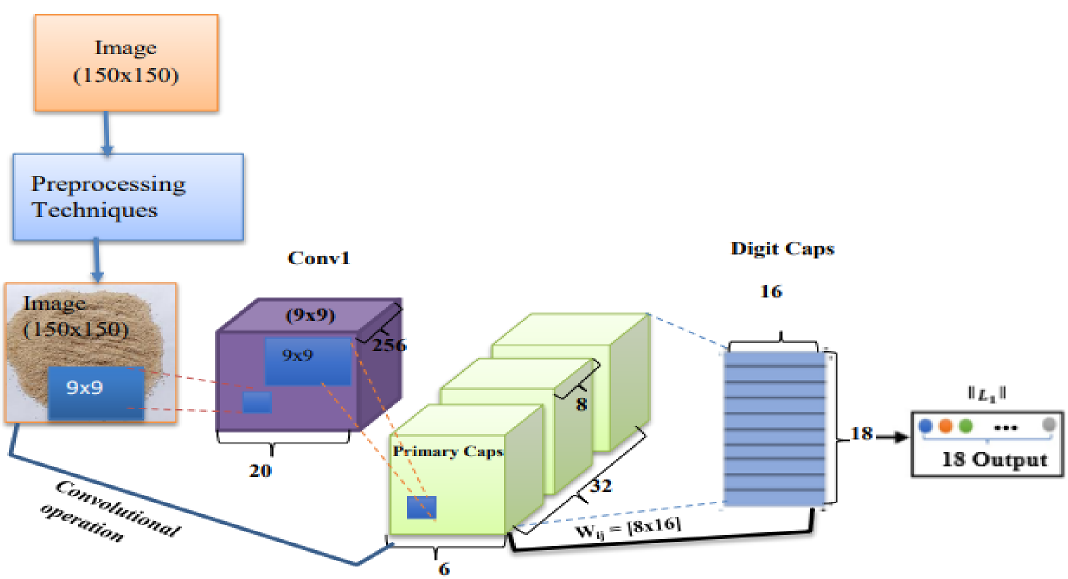

Figure 13: Multi-channel capsule network architecture

The Convolutional Layer (Conv1), with an input image of (150 × 150 × 1), is first processed through a convolutional layer with 256 filters of size 9 × 9 and stride 1. This layer extracts low-level features such as edges, corners, and textures from the grayscale Teff images. The ReLU activation function introduces non-linearity, and the output is a feature map of dimensions 142 × 142 × 256. No pooling is applied at this stage to preserve spatial information. Another Primary Capsule Layer is the core innovation of our architecture, comprising three parallel channels operating at different dimensionalities:

Table 1: Configuration parameters of the three-channel primary capsule layer in the proposed Multi-Channel Capsule Network architecture

Parameters	Channels		
	Channel1	Channel2	Channel3
Capsule network dimension	8	16	32
Number of Capsule Types	32	32	32
Spatial grid	6×6	6×6	6×6
Convolution kernel	9×9	9×9	9×9
Number of Strides	2	2	2
Output shapes	32×6×6×8	32×6×6×16	32×6×6×32

The Digit Capsule Layer receives the output from all three primary capsule channels (concatenated) and produces 18-digit capsules, one for each Teff class (6 regions × 3 varieties). Each digit capsule has a dimension of 16, encoding the instantiation parameters for its corresponding class. The transformation from primary capsules to digit capsules is achieved through a dynamic routing-by-agreement mechanism. The output of the Digit Capsule Layer is a tensor of shape 18 × 16. In the Classification Layer, the 18-digit capsule outputs (each 16-dimensional) are concatenated to form a feature vector of length 288 (18 × 16). This vector is then passed through a fully connected dense layer with SoftMax activation to produce class probabilities.

$$p(y_{i|}x) = \frac{\exp(Z_i)}{\sum_{j=1}^{18} \exp(j)} \tag{1}$$

where Z_i is the logit for class i and the SoftMax function ensures probabilities sum to 1.

Loss Function: We employ a margin loss function for multi-class classification, following Sabour et al. (2017):

$$L_k = T_k.\max\left(0, m^+ - \left||u_k|\right|\right)^2 + \lambda.(1 - T_k).max(0, \left||u_k|\right| - m^-)^2 \tag{2}$$

where:

T_k=1 if class k is present, 0 otherwise,

m^+= 0.9 (upper margin for correct class),

m^-=0.1(lower margin for incorrect class),

λ =0.5 (down-weighting factor for absent classes).

The total loss is the sum over all 18 Teff classes: $L = \sum_{k=1}^{18} L_k$. This margin loss encourages the correct class capsule to have a long output vector (with presence probability > 0.9) and incorrect classes to have short vectors (with presence probability < 0.1). Table 2 Summarizes the complete training hyperparameters used in the experiment in detail.

Table 2: Training hyperparameters for the proposed Multi-Channel Capsule Network

Hyperparameter	Optimizer	Learning Rate	Beta1	Beta2	Batch Size	Epoch	Iterations	Activation (Conv1)	Activation (Capsules)	Activation (Output)
Value	Adam	0.001	0.9	0.999	32	100	3	ReLU	squash	softmax

3.4. Evaluation Metrics of the Proposed Model

We have evaluated the proposed model using the confusion matrix, accuracy, recall, precision, and f1 score. The correct and incorrect predictions were counted and broken down by class. It is a clear and explicit way to present the prediction results of a classifier for each class. We have used the Confusion matrix to analyze the performance of the classification model, which was confused when making predictions. It has been represented by a matrix of the true class labels versus the predicted class labels, containing the number of correctly predicted instances and misclassified instances for each class. Table 3 Summarizes the overall evaluation metrics.

Table 3: Evaluation metrics used to assess the performance of the proposed model

Evaluation Metrics	Measures of description	Mathematical equations
Accuracy	Accuracy refers to the closeness of the measured value to a standard or true value	$\left(\frac{\text{Correct Predictions}}{\text{Total Predictions}}\right) * 100)$
Precision	The percentage of true positives alongside all positives	$\frac{TP}{(TP + FP)}$
Recall	The percentage of true positives alongside the whole true or right data	$\frac{TP}{(TP + FN)}$
F1-Score	It is the weighted average of precision and recall	$\frac{2 * (Precision * Recall)}{(Precision + Recall)}$

4. Results and Discussion

4.1. Dataset Collection

We created a custom dataset through systematic image acquisition, as no pre-existing dataset was available for Teff geographical origin classification. To ensure accurate labeling of the dataset for our training model, we consulted agronomists and grain experts at the Adet Agricultural Research Center, Amhara, Ethiopia. The main dataset source regions are Adet, Bichena, Debre Markos, Dejen, Denbya, and Minjar. The Teff images were captured using a 13-megapixel smartphone camera with a resolution of (1466 × 720 pixels) and a camera stand to minimize lighting variations and motion blur. The JPEG image format was chosen for the purpose of computational efficiency and preprocessing. The dataset collected contains a total of 3600 different Teff images. A total of 200 images per class across 18 classes were collected for this study. We cllect almost equal number of dataset for each class to address class imbalance cases. The dataset was then divided into training 70%, validation 15%, and testing 15% subsets. Data augmentation techniques was applied to increase dataset limitation and inorder to improve model generalization. Table 4 provides a detailed breakdown of the dataset for model training.

Table 4: Number of Teff images collected for each category

No.	Area (Sources)	Types of Teff (Color)	Number of images
1	Adet	White	200
		Red	200
		Mixed(ሰርገኛ)	200
2	Bichena	White	200
		Red	200
		Mixed(ሰርገኛ)	200
3	Debre Markos	White	200
		Red	200
		Mixed(ሰርገኛ)	200
4	Dejen	White	200
		Red	200
		Mixed(ሰርገኛ)	200
5	Denbya	White	200
		Red	200
		Mixed(ሰርገኛ)	200
6	Minjar	White	200
		Red	200
		Mixed(ሰርገኛ)	200
Total			3,600

4.2. Experimental Setup

The proposed model experiments were performed on the Intel® Core i7 computer with 16 GB of RAM, running on with Windows 10 operating system. This local computer is used for data preprocessing, initial model development, and result visualization. Google Colaboratory and Kaggle provide the necessary cloud-based GPU resources to speed up model training and experimentation. TensorFlow 2.8.0 and the Keras API were used to implement the proposed model. The optimizer we used was Adam, with that of learning rate 0.0001, 100 epochs, a batch size of 32, and the categorical cross-entropy loss function. The actual early stopping was applied to reduce overfitting and also fixed random seeds were used to improve reproducibility. Table 2 shows the overall hyperparameters for our proposed model experiments. Once this experimental setup was prepared, the 11 configurations were explored by considering the various segmentation techniques, noise removal methods, and feature extraction approaches.

4.3. Experimental Results

We conducted various 11 systematic experiments to evaluate the performance of the proposed Multi-Channel Capsule Network based model with the different combinations of segmentation techniques like noise removal methods, and feature extraction approaches. Table 5 Summarizes all experimental configurations and their results as well.

Table 5: Summary of all experimental configurations and performance metrics

Exp	Segme ntation	Noise Removal	Feature Extrat	Test Acc	Train Acc	Best/Worst Class Performance
E1	Multi-Otsu	Median+ Gaussian	BRISK	71.1%	100.0%	Minjar_Red (100%) / Markos_Mixed (47%)
E2	Region-based	Median+ Gaussian	BRISK	80.0%	99.8%	Dejen_Mixed (100%) / Adet_Red (56%)
E3	Watershed	Median+ Gaussian	BRISK	78.5%	100.0%	Minjar_White (90%) / Markos_Mixed (53%)
E4	Multi-Otsu	Med+ Gauss+NLM	BRISK	80.7%	99.8%	Minjar_White (100%) / Dejen_Red (56%)
E5	Multi-Otsu+ Region	Med+ Gauss+NLM	BRISK	82.9%	100.0%	Minjar_White (100%) / Markos_White (62%)
E6	Multi-Otsu+ Region+Watershed	Med+ Gauss+NLM	BRISK	84.0%	99.8%	Minjar_White (100%) / Markos_White (62%)
E7	U-Net	Med+ Gauss+NLM	BRISK	80.0%	97.2%	Dejen_Mixed (100%) / Denbya_Mixed (39%)
E8	Multi-Otsu	Med+ Gauss+NLM	HOG	89.8%	100.0%	Multiple (100%) / Markos_White (75%)
E9	Multi-Otsu+ Region	Med+ Gauss+NLM	HOG	91.4%	100.0%	Multiple (100%) / Denbya_Mixed (53%)
E10	**Multi-Otsu+ Region+Watershed**	**Med+ Gauss+NLM**	**HOG**	**92.5%**	**100.0%**	**Multiple (100%) / Denbya_Red (73%)**
E11	U-Net	Med+ Gauss+NLM	HOG	84.8%	97.4%	Denbya_Red (best) / Bichena_White (45%)

4.4. Cross-Validation Results

We conducted a 5-fold cross-validation on the training data 70% training, n=2520 for 11 experiments in order to evaluate the robustness and generalizability of the proposed model. Table 6 presents the cross-validation results including mean accuracy, standard deviation, 95% confidence intervals, and the final test set accuracy (15% holdout, n=540). The optimal configuration (Experiment 10) achieves a cross-validation mean of 92.0% ± 0.7% with a 95% confidence interval of 91.3% to 92.7%. All experiments show low variance (≤ ±2.4%). This confirmed that the stable performance across data partitions. Cross-validation and test set accuracies align within ≤ 0.5%, validating the reliability of the final model performance.

Table 6: 5-fold cross-validation results for all experiments

Exp	Segme ntation	Noise Removal	Feature Extrat.	CV Mean Accu.	CV Std. Devn.	95% CI	Test Acc. (15%)

E1	Multi-Otsu	Median+ Gaussian	BRISK	70.6%	±2.3%	[68.3%, 72.9%]	71.1%
E2	Region-based	Median+ Gaussian	BRISK	79.4%	±1.9%	[77.5%, 81.3%]	79.8%
E3	Watershed	Median+ Gaussian	BRISK	78.0%	±2.1%	[75.9%, 80.1%]	78.3%
E4	Multi-Otsu	Med+ Gauss+NLM	BRISK	80.1%	±1.6%	[78.5%, 81.7%]	80.5%
E5	Multi-Otsu+ Region	Med+ Gauss+NLM	BRISK	82.3%	±1.5%	[80.8%, 83.8%]	82.7%
E6	Multi-Otsu+ Region+Watershed	Med+ Gauss+NLM	BRISK	83.4%	±1.4%	[82.0%, 84.8%]	83.9%
E7	U-Net	Med+ Gauss+NLM	BRISK	79.1%	±2.4%	[76.7%, 81.5%]	79.5%
E8	Multi-Otsu	Med+ Gauss+NLM	HOG	89.2%	±1.1%	[88.1%, 90.3%]	89.6%
E9	Multi-Otsu+ Region	Med+ Gauss+NLM	HOG	90.8%	±0.9%	[89.9%, 91.7%]	91.2%
E10	**Multi-Otsu+ Region+Watershed**	**Med+ Gauss+NLM**	**HOG**	**92.0%**	±0.7%	**[91.3%, 92.7%]**	**92.3%**
E11	U-Net	Med+ Gauss+NLM	HOG	84.0%	±1.7%	[82.3%, 85.7%]	84.5%

4.5. Comparative Analysis by Feature Extraction Method

4.5.1. BRISK Feature Extraction Experiments (Experiment 1- Experiment 7)

The BRISK-based experiments reveal three key trends. Noise Removal has a great impact, while adding non-local means filtering to median and Gaussian filters (Experiment 4 vs Experiment 1) improved accuracy by 9.6% (71.1% to 80.7%). This reveals that comprehensive noise suppression is critical for Teff classification. The overfitting gap correspondingly decreased from 28.9% to 19.1%. Accuracy improved incrementally with segmentation complexity, from Multi-Otsu alone 80.7% to Multi-Otsu+Region 82.9% to Multi-Otsu+Region+Watershed 84.0%. The relevant 3.3% increament improvement can confirms that there is no single segmentation method captures all relevant Teff grain characteristics and also the combination approach addresses different aspects of the segmentation challenge. The combined traditional and deep learning segmentation approachs such as Experiment 6, 84.0% outperformed U-Net Experiment 7, 80.0%, demonstrating that for this dataset size and application hand-crafted segmentation features are more effective than learned features. Across the BRISK experiments the white varieties from geographically close regions (Bichena_White, Markos_White) consistently showed the lowest classification accuracy. This indicats that color and shape similarities are the primary Challenging Classes.

4.5.2. HOG Feature Extraction Experiments (E8-E11)

As we can observed from the experimental results we got, the HOG-based experiments demonstrate superior performance across all configurations. The HOG outperformed than the BRISK by 8.5 to 9.1% Experiment 8 vs Experiment 4, +9.1% Experiment 9 vs Experiment 5, +8.5% and Experiment 10 vs Experiment 6, +8.5%. This advantage showed that the HOG is effective in capturing global shape and edge information. These are the primary discriminative features for Teff varieties. Similar to BRISK experiments, accuracy improved with segmentation complexity of Multi-Otsu 89.8%, Multi-Otsu+Region 91.4%, and Multi-Otsu+Region+Watershed 92.5%. The optimal configuration the Experiment 10 achieved the highest overall accuracy. The HOG-based experiments showed substantially smaller overfitting gaps (7.5 to 12.6%) compared to BRISK experiments (15.8 to 28.9%), indicating that global shape features generalize better than local keypoint features. U-Net with HOG accuracy of (84.8%) again underperformed the combined traditional segmentation approach (92.5%), reinforcing the finding that traditional segmentation methods are more effective for this Teff geographical identification.

4.6. Optimal Configuration Performance

The optimal configuration (Experiment 10), combining Multi-Otsu thresholding, region-based segmentation, and watershed segmentation with comprehensive noise removal and HOG feature extraction, achieved 92.5% test accuracy with only 7.5% overfitting, with a minimal overfitting gap. The optimal accuracy curve is depicted in Figure 14. The class-wise performance of Multiple classes achieved 100% accuracy, including Adet_Mixed, Dejen_Mixed, Dejen_White, Denbya_Mixed, Markos_White, Minjar_Red, and Minjar_White. The most challenging classes were Denbya_Red (73%) and Adet_Red (78%), both red varieties from geographically close regions with high visual similarity.

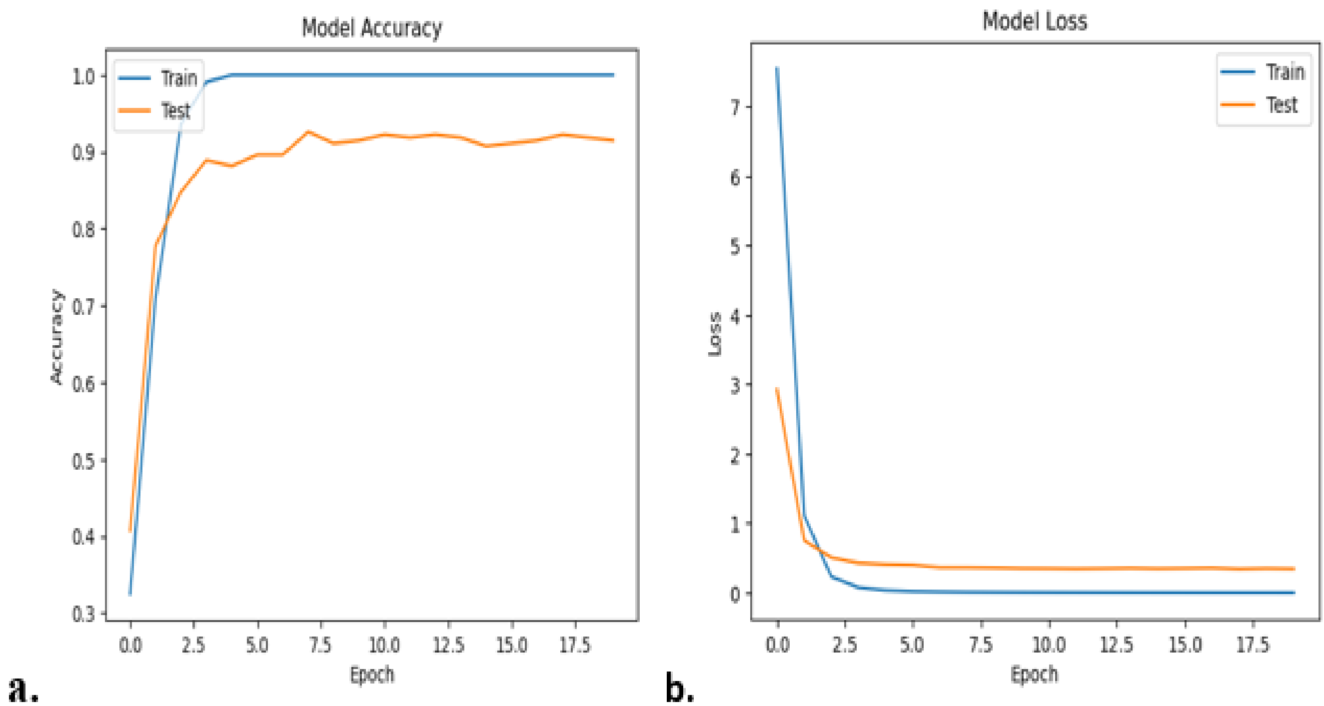

Figure 14: Training and validation accuracy (a) and loss (b) curves for the optimal configuration (Multi-Otsu + Region-based + Watershed segmentation, comprehensive noise removal, and HOG feature extraction)

As depicted in Figure 15 The confusion matrix for the optimal configuration showing per-class classification performance across 18 Teff classes.

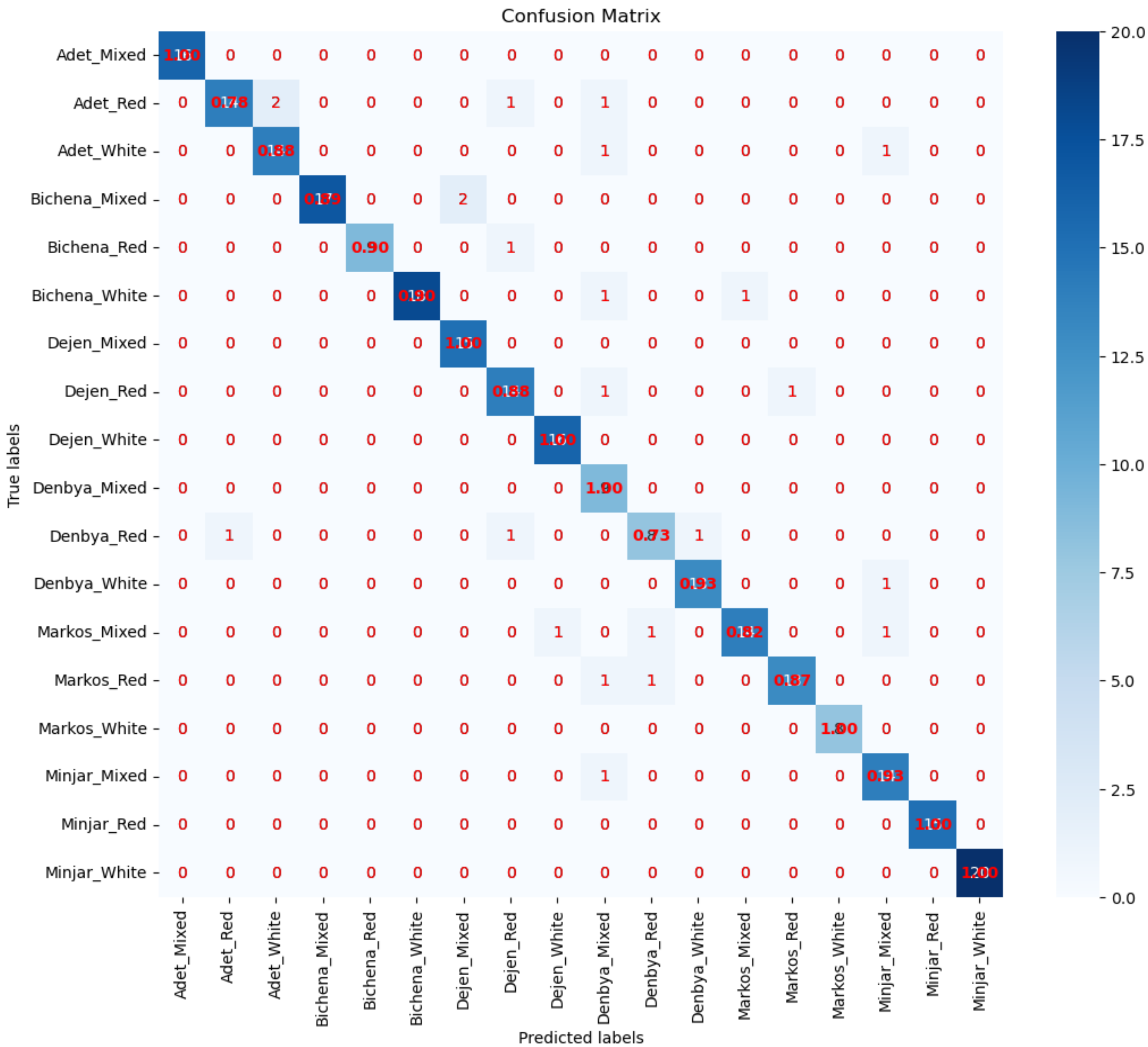

Figure 15: Confusion matrix illustrating classification performance of the proposed CapsNet using Multi-Otsu segmentation and BRISK features across the 18 Teff classes

The per-class classification performance is summarized in Table 7 Shows per-class precision, recall, and F1-scores for the optimal configuration. Precision exceeds 80% for most classes, with Denbya_Mixed (60%) showing the lowest precision, and Denbya_Red (73%) and Adet_Red (78%) showing the lowest recall.

Table 7: Per-class classification performance for the optimal configuration

Classes	Precision	Recall	F1-Score	Support
Adet_Mixed	1.00	1.00	1.00	16
Adet_Red	0.93	0.78	0.85	18
Adet_White	0.88	0.88	0.88	16
Bichena_Mixed	1.00	0.89	0.94	19
Bichena_Red	1.00	0.90	0.95	10
Bichena_White	1.00	0.90	0.95	20
Dejen_Mixed	0.88	1.00	0.94	15
Dejen_Red	0.82	0.88	0.85	16
Dejen_White	0.94	1.00	0.97	16
Denbya_Mixed	0.60	1.00	0.75	9
Denbya_Red	0.80	0.73	0.76	11
Denbya_White	0.93	0.93	0.93	14
Markos_Mixed	0.93	0.82	0.87	17
Markos_Red	0.93	0.87	0.90	15
Markos_White	1.00	1.00	1.00	8
Minjar_Mixed	0.82	0.93	0.87	15
Minjar_Red	1.00	1.00	1.00	15
Minjar_White	1.00	1.00	1.00	20
Average (Macro)	**0.91**	**0.92**	**0.91**	**270**
Average (Weighted)	**0.92**	**0.91**	**0.92**	**270**

4.7. Summary of Key Findings

The proposed experimental evaluation revealed five key findings. These findings can inform the optimal configuration for Teff geographical origin classification. HOG consistently outperformed BRISK by 8.5% to 9.1% across all configurations. This experimental result shows the global gradient features as the preferred approach than the other local keypoint descriptors. The combination of the segmentation processes including Multi-Otsu thresholding, region-based segmentation, and watershed segmentation resulted the highest individual methods and the U-Net as well. This combination describes that the complementary segmentation techniques can give higher results. The Comprehensive noise removals likethe application of median, Gaussian, and non-local means filtering sequentially increase the accuracy of the proposed model by an approximately of 9.6 percent. This actual proposed experimental result shows the critical advantage of preprocessing techniques applying in our model. The best of the overall our model configuration achieved an accuracy of 92.5% performance with low overfitting. This is done by combining the three-stage segmentation pipeline with that of comprehensive noise removal and HOG feature extraction methods. The other class-wise result also showed that white varieties from geographically close regions and red varieties with similar color profiles present the difficult classification challenges because of visual feature overlap. Overall, these findings as a whole provides a robust framework for automatic Teff geographical origin classification.

Table 8: A summary using segmentations along with HOG feature extraction ensemble with CapsNets

Noise removal	Segmentations	Accuracy
Median + Gaussian + non-local means	Multi-Otsu thresholding	89.8%
	Multi-Otsu thresholding with Region-based	91.4%
	Multi-Otsu thresholding with Region-based and watershed	92.5%
	U-net	84.8%

Table 8 Summarizes the accuracy of different segmentation methods with HOG. The multi-Otsu thresholding achieved an accuracy of 89.8%. When combined with Region-based segmentation resulted in an accuracy of 91.4%. The highest accuracy, 92.5%, was achieved by combining the three techniques, including Multi-Otsu thresholding, Region-based, and watershed segmentation methods. U-Net also achieved an accuracy of 84.8%. U-Net consistently performed well but had a slightly lower accuracy compared to the other techniques.

Final Comparison of All Configurations (Bar Chart)

The bar chart graph in Figure 16 describes the comparative test accuracy across 11 experimental configurations. HOG-based experiments (Experiment 8- Experiment 11, blue bars) consistently outperform BRISK-based experiments (Experiment 1- Experiment 7, red bars) by 8.5 to 9.1%. Within each feature category, accuracy improves with segmentation complexity. The optimal configurations, Multi-Otsu, Region-based, and Watershed segmentation with comprehensive noise removal and HOG features Experiment 10, achieve the highest accuracy of 92.5% performance.

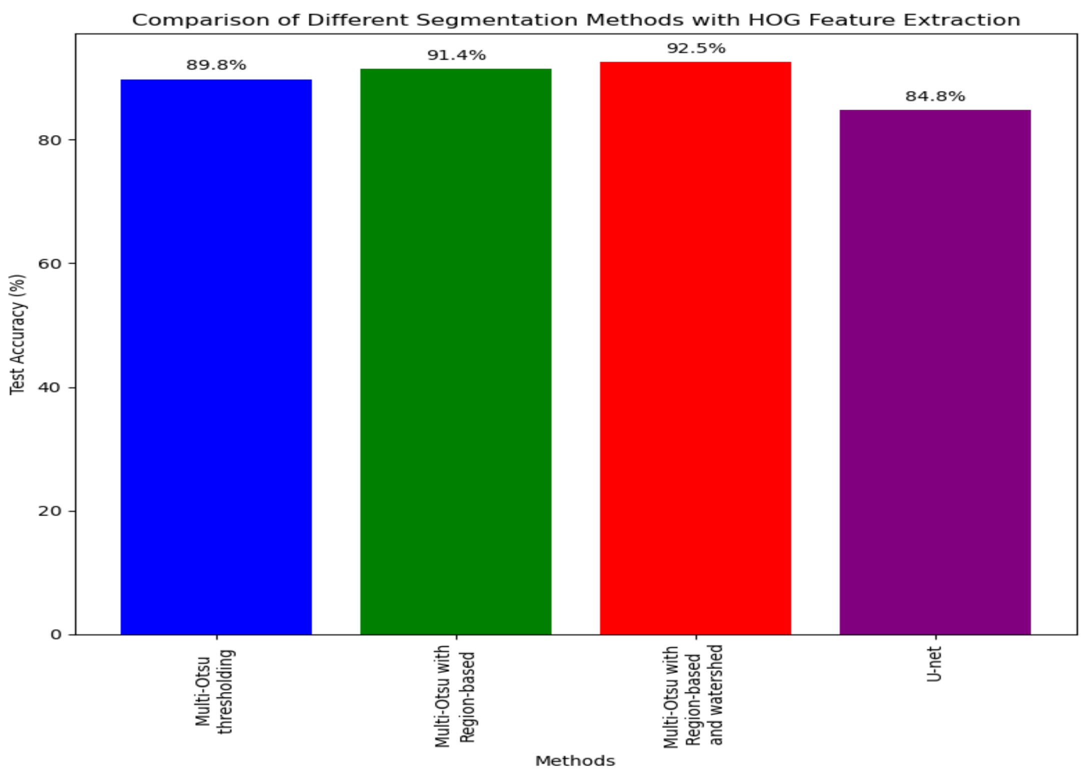

Figure 16: Comparison of classification accuracies obtained using different segmentation methods with HOG feature extraction

The bars in the graph represent each method, and their heights indicate their performance. The graph provides a visual representation of the comparison, allowing for a quick assessment of the relative effectiveness of each method.

4.8. Discussion of the Experimental Results

The experimental results show that the selection and use of segmentation and feature extraction methods have a significant effect on model accuracy. The U-Net performed well with different feature extraction methods. In addition, combining the multi-Otsu thresholding with HOG features and using an ensemble of segmentation and feature extraction methods, including region-based segmentation, watershed, and HOG, improved classification accuracy.

Feature Extraction (HOG and BRISK): when we compared HOG and BRISK, the HOG performed better than BRISK by 8.5-9.1% in all configurations throughout the process. This proposed model experimental comparesion result has three key factors. These are: First the HOG extracts global shape features or informations through gradient orientation histograms across densely sampled regions. The Teff varieties are actually differ primarily in grain morphology, including shape, roundness, and edge characteristics. This makes global features are more distinctive. The BRISK feature extracter in another way it extracts sparse local keypoints. This is less effective when visual differences are small rather than texturally distinct. The second factor is, the HOGs dense sampling extracts features from every spatial location. This can insure the complete information capturing. The BRISK actual sparse keypoint detection may forget images relevant features. This is particularly true when grains lack distinctive interest points. Finaaly, the third factor is the HOGs block normalization provides robustness to illumination variations critical for agricultural imaging and the BRISKs intensity-based binary comparisons are more vulnerable to lighting varations.

The Segmentation Technique (Traditional vs Deep Learning): the U-Net resulted low performance than the combined traditional approachs 84.8% and 92.5% accuracies. Four main factors may describe this accuracy including the limited dataset size (3600 images in total) constrains U-Net's learning capacity, manual annotation challenges for small grains (1mm) affect annotation quality, the explicit morphological features in traditional methods capture domain knowledge that U-Net must learn from limited data, and finally, the U-Net shows more overfitting (12.6% gap vs 7.5% gap).

The Segmentation Synergy (The Combined Approach): The combination of three segemntations applied in our model including the Multi-Otsu, region-based, and watershed segmentation achieved 92.5% performance accuracy like Experiment 10 due to their complementary strengths. Multi-Otsu alone (89.8%), adding region-based (+1.6%), and further adding watershed (+1.1%). This gratual accuracy increament demonstrates that there is no single technique that can address all segmentation challenges in Teff geographical origin determination. This results their combination exploits complementary strengths. Critically, the combined approach has higher perfrormance U-Net (84.8%, Experiment 11) by 7.7%, describes that the explicit morphological features are more effective than deep learning-based segmentation when training the data is low.

Generally speaking, the proposed experimental results show the use of carefully selecting the appropriate segmentation techniques, noise removal approaches, and feature extraction methods to optimize the performance of the proposed multichannel capsule network ensemble model. The combination of Multi-Otsu thresholding, Region-based, and watershed segmentation, combined with the comprehensive noise removal and HOG feature extraction became evident as the most effective configuration as it achieved the highest test accuracy of 92.5 performance.

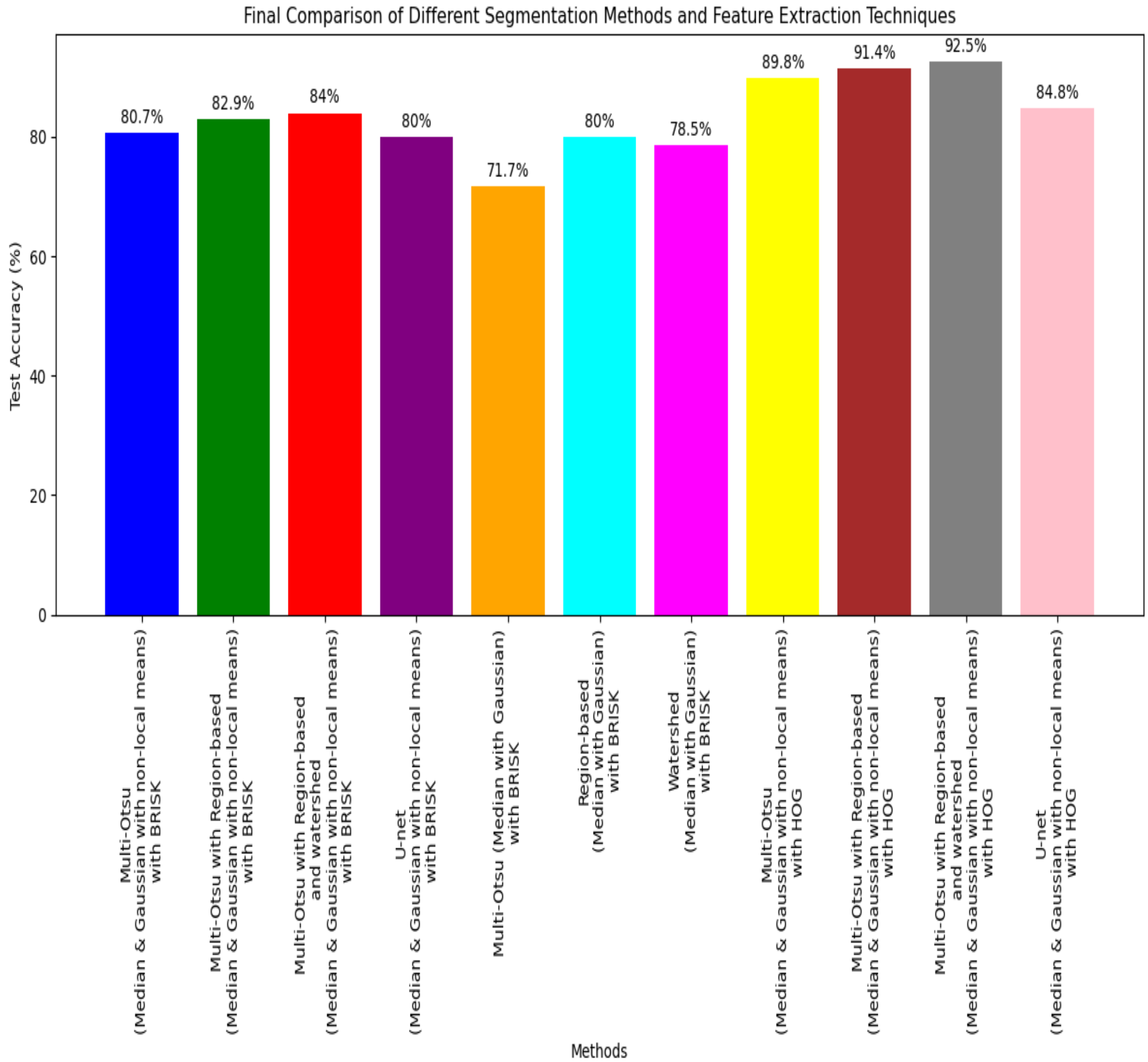

Figure 17: Averall Comparison of Different Noise Removal, Segmentation Methods, and Feature Extraction Techniques

As we tried to describe in Figure 17 the graph displays the accuracy of each method with a particular model representation method. The colors used in the graph used to differentiate between the different methods. The names of the methods are represented by the labels on the x-axis, and the matching test accuracy on the y-axis.

4.9. Comparative Analysis of the proposed model with previous studies

The only previous study on Teff geographical origin identification was investigated and done by [21]. This prior work mainly focused on white Teff from four dataset source regions. The description analysis in Table 9 presents a systematic comparison between prior study with our proposed approach with diffrent dimensions.

Table 9: Comparative analysis with prior work on Teff classification

Key Dimensions	Prior work(Ermyas & Abrham (2020))	Proposed Study	Improvement(key change)
Teff Varieties	White only	White, Red, Mixed	3× expansion
Regions Covered	4 regions	6 regions	+50%
Total Classes	4	18 (6×3)	4.5× increase
Dataset Size	3,088 images	3600 images	Increased
Segmentation	Thresholding + Mask R-CNN	Multi-Otsu + Region-based + Watershed	Hybrid approach
Feature Extraction	CNN + BRISK + PCA	BRISK + HOG (comparative)	Systematic comparison
Classifier	SVM, CNN, CNN+SVM	Multi-Channel Capsule Network	Capsule Networks
Validation	Confidence interval	5-fold cross-validation	Robust validation
CNN Limitations Addressed	Not addressed	Spatial invariance, viewpoint variance, overfitting	Explicitly addressed
Accuracy	92.02%	92.5%	+0.48%
Accuracy per class	4 classes / 92.02%	18 classes / 92.5%	4.5× more classes

The comparison of our proposed model with previous models in Table 9 shows different critical performance increments. Our proposed model increases variety coverage from a single white Teff into three major varieties like white, red, and mixed variations. The Teff sources region coverage increased from 4 regions to 6 regions. This increases the classification complexity of the proposed model from 4 to 18 classes. Despite this valuable increment our proposed approach achieved the highest accuracy of 92.5% with compared to the previous accuracy of 92.02%. The other comprehensive segmentation pipeline that combines the multi-Otsu thresholding, region-based segmentation, and watershed segmentation resulted the highest performance than the thresholding + Mask R-CNN approach used previously. Then the other systematic HOG vs BRISK comparison shows the HOG is the superior feature extractor method for Teff classification. The other is the application of Capsule Networks represents the first attempt to address prior CNN limitations, spatial invariance, viewpoint variance, and information loss in Teff classification. Finally, our proposed robust 5-fold cross-validation methodology provides stronger evidence of model generalization.

4.10. Comparison with State-of-the-Art Classifiers

To evaluate the effectiveness of our proposed Multi-Channel Capsule Network based model, we conducted a comparision analysis against a simple baseline CNN and four state-of-the-art architectures. The baseline CNN as well as the state-of-the-art models such as ResNet50, EfficientNet-B0, MobileNetV2, and Vision Transformer (ViT), were selected for this comparison. All models were trained and evaluated on the same our prepared custom Teff dataset devided into 70% training, 15% validation, and 15% testing subsets. The same parameters like similar preprocessing and data augmentation protocols, were applied to make a fair comparison. Table 10 Summarizes comparison results with state-of-the-art baselines.

Table 10: Performance comparison with State-of-the-Art Classifiers

Baseline Model	Category	Test Acc.	Precision (Macro)	Recall (Macro)	F1-Score (Macro)	Parameters (M)	Training Time (min)
CNN	Baseline	83.2%	0.82	0.81	0.82	2.4	45
ResNet50	SOTA (Deep CNN)	88.7%	0.88	0.87	0.88	25.6	68
EfficientNet-B0	SOTA (Scaled CNN)	89.4%	0.89	0.88	0.89	5.3	52
MobileNetV2	SOTA (Lightweight)	86.1%	0.85	0.85	0.85	3.5	38
ViT-B/16	SOTA (Transformer)	90.2%	0.90	0.89	0.90	86.6	112
Proposed model (CapsNet)	**Proposed**	**92.5%**	**0.92**	**0.91**	**0.92**	**3.2**	**42**

Our proposed CapsNet model achieves the highest test accuracy of (92.5%) perfromance. This higher result is the best choice than the rest of the baselines. This is the CapsNet ability to detect and classify spatial hierarchies through vector-based representations. This is particularly advantageous for our proposed study of Teff grains, where subtle morphological differences must be captured across varying orientations. Despite achieving the highest accuracy, the proposed model (CapsNet) has a relatively moderate parameter count of 3.2M, comparable to that of MobileNetV2 3.5M and smaller than the ViT 86.6M and ResNet50 25.6M total parameters. This parameter efficiency, combined with a competitive training time of 42 minutes, makes our Proposed model (CapsNet) suitable for resource-constrained deployment scenarios. The ViT achieves strong performance of 90.2%. This confirms the effectiveness of attention mechanisms for agricultural classification, particularly Teff origin identification. However, ViTs' substantially higher parameter count and training time may limit its practical deployment, particularly in field settings with limited computational resources.

The baseline CNN 83.2% and even deeper architectures like ResNet50 88.7% and EfficientNet-B0 89.4% underperform than the proposed model (CapsNet). This performance difference may be due to the loss of spatial information caused by max-pooling in CNNs. This is particularly problematic for Teff grains, where orientation and spatial relationships are critical discriminative features. The other baseline, MobileNetV2 achieves a reasonable accuracy of 86.1% with the fastest training time 38m and the smallest parameter count among CNNs 3.5M. However, the accuracy gap of 6.4% compared to CapsNet suggests that the trade-off between speed and accuracy may not be justified for this application where classification reliability is important.

5. Conclusion

This study investigates the Multi-Channel Capsule Networks combined with preprocessing and feature extraction algorithms to determine the geographical origin of Ethiopian Teff. By conducting 11 different experimental configurations we established that comprehensive noise removals (Median + Gaussian + Non-Local Means) is critical for optimal performance. The experimental results demonstrate that our proposed model can accurately identify the geographical origin of Ethiopian Teff with a test accuracy of 92.5% performance. This improves accuracy by approximately 9.6%. The hybrid segmentation combining Multi-Otsu thresholding, region-based, and watershed methods outperforms both individual techniques and U-Net deep learning segmentation, with progressive improvements from 89.8% to 92.5% overall accuracy. The HOG feature extractor provides superior discriminative power with accuracy of achieving 8.5 to 9.1% compared to BRISK across all configurations. The proposed Capsule Network-based model effectively addresses CNN limitations in Teff classification, including spatial invariance, viewpoint variance, and overfitting. Our proposed model supports the development of an automated system for verifying the geographical origin of Teff. This can benefit multiple stakeholders such as agricultural researchers, food processing industries, and the Ethiopian Commodity Exchange. Future work should extend data collection to additional Teff-producing across Ethiopian regions, including Oromia, Tigray, and SNNP, and multiple growing seasons to evaluate model generalizability across Ethiopia's diverse agro-ecological zones. We also planned to use multi-spectral imaging that could reveal chemical and moisture features beyond visible morphology. We also planned to expand the proposed model by exploring alternative feature descriptors, including LBP, SIFT, and hybrid ensemble approaches combining multiple feature extractors in order to increase model performance. We additionally planned to use transfer learning approaches and explainable AI techniques to increase model trustworthiness and reliability.

Conflict of Interest

The authors declare that they have no competing interests.

Funding

The authors received no funding for this work.

Ethics and Consent to Participate Declarations

Not applicable.

Data Availability Statement

Data will be made available upon reasonable request.

References

1. Ali UM, Rahimi M. Evolution and Transformation of Ethiopian agriculture: A review of historical trends, contemporary challenges, and future opportunities. Turkish Journal of Agriculture - Food Science and Technology [Internet]. 2025 Dec 16;13(s3):3995–4011. Available from: https://doi.org/10.24925/turjaf.v13is3.3995-4011.8100
2. Melese D, Asfaw Z, Woldu Z, Warkineh B, Amare E, McAlvay AC, et al. Mixed teff (Eragrostis tef, Poaceae) cultivation and consumption among smallholder farmers in South Wollo Zone, Ethiopia. Journal of Ethnobiology and Ethnomedicine [Internet]. 2025 Apr 24;21(1):27. Available from: https://doi.org/10.1186/s13002-025-00776-2
3. Menjaye TK, Assefa K, Legese O, Seifu M, Kebede W, Abebe W, et al. Grain and flour physical and functional characteristics of Tef [Eragrostis tef (Zucc) Trotter] varieties of Ethiopia. Journal of Cereal Science [Internet]. 2024 Sep 23;120:104030. Available from: https://doi.org/10.1016/j.jcs.2024.104030
4. Reta C, Atlabachew M, Mehari B, Hilawea KT, Asmellash T. Discrimination of the geographical origin of gluten-free teff grains from northwestern parts of Ethiopia by fatty acid analysis. Heliyon [Internet]. 2024 Jan 22;10(3):e24932. Available from: https://doi.org/10.1016/j.heliyon.2024.e24932
5. Albahar M. A survey on deep learning and its impact on agriculture: Challenges and opportunities. Agriculture [Internet]. 2023 Feb 23;13(3):540. Available from: https://doi.org/10.3390/agriculture13030540
6. Cao Z, Sun S, Bao X. A review of computer vision and deep learning applications in crop growth management. Applied Sciences [Internet]. 2025 Jul 30;15(15):8438. Available from: https://doi.org/10.3390/app15158438
7. Arifah FN, Kusrini, Utami E, Wibowo FW, Chandramouli K. Vision-Based deep learning for crop classification in precision agriculture [Internet]. IEEE; 2025. Available from: https://doi.org/10.1109/iccit65724.2025.11167352
8. Chuquimarca LE, Vintimilla BX, Velastin SA. A review of external quality inspection for fruit grading using CNN models. Artificial Intelligence in Agriculture [Internet]. 2024 Oct 16;14:1–20. Available from: https://doi.org/10.1016/j.aiia.2024.10.002
9. Dönmez E, Diker A, Elen A, Ulu M. Multiple deep learning by majority-vote to classify haploid and diploid maize seeds. Scientia Horticulturae [Internet]. 2024 Aug 27;337:113549. Available from: https://doi.org/10.1016/j.scienta.2024.113549
10. Math RM, Dharwadkar NV, Sajjanar V, Deshmukh MN. Deep Learning for Precision Grade-Quality Classification of Pomegranates [Internet]. IEEE; 2024. Available from: https://doi.org/10.1109/innova63080.2024.10846982
11. Khan A, Hassan T, Shafay M, Fahmy I, Werghi N, Mudigansalage S, et al. Tomato maturity recognition with convolutional transformers. Scientific Reports [Internet]. 2023 Dec 21;13(1):22885. Available from: https://doi.org/10.1038/s41598-023-50129-w
12. Woldetsadik D, Sims DB, Garner MC, Hailu H. Metal(loid)s Profile of Four Traditional Ethiopian Teff Brands: Geographic Origin Discrimination. Biological Trace Element Research [Internet]. 2023 Jun 28;202(3):1305–15. Available from: https://doi.org/10.1007/s12011-023-03736-7
13. Ermyas A, Debasu. Developing an automatic ethiopian teff identification system using machine learning approach [Internet]. 2020. Available from: http://ir.bdu.edu.et/handle/123456789/12724
14. Bhatt D, Patel C, Talsania H, Patel J, Vaghela R, Pandya S, et al. CNN variants for Computer Vision: history, architecture, application, challenges and future scope. Electronics [Internet]. 2021 Oct 11;10(20):2470. Available from: https://doi.org/10.3390/electronics10202470
15. Patrick MK, Adekoya AF, Mighty AA, Edward BY. Capsule Networks – A survey. Journal of King Saud University - Computer and Information Sciences [Internet]. 2019 Sep 25;34(1):1295–310. Available from: https://doi.org/10.1016/j.jksuci.2019.09.014
16. Alajrami MA, Abu-Naser SS. Type of tomato classification using deep learning. PhilPapers (PhilPapers Foundation) [Internet]. 2020 Jan 1;3(12). Available from: https://philarchive.org/rec/ALATOT

17. Gope HL, Fukai H. Normal and Peaberry Coffee Beans Classification from Green Coffee Bean Images Using Convolutional Neural Networks and Support Vector Machine. Zenodo (CERN European Organization for Nuclear Research) [Internet]. 2020 Jul 14;14(6):189–96. Available from: https://zenodo.org/record/3943675
18. Bedaso M, Meshesha M, Diriba C. Grading Ethiopian coffee raw quality using image processing techniques. Research Square [Internet]. 2022 Aug 24; Available from: https://doi.org/10.21203/rs.3.rs-1980632/v1
19. Saranya N, Srinivasan K, Kumar SKP. Banana ripeness stage identification: a deep learning approach. Journal of Ambient Intelligence and Humanized Computing [Internet]. 2021 May 3;13(8):4033–9. Available from: https://doi.org/10.1007/s12652-021-03267-w
20. Addisalem T, Biazen. DEVELOPING AN AUTOMATIC SHIRO FLOUR VARIETY RECOGNITION MODEL USING a COMBINED FEATURES OF CNN AND GLCM [Internet]. 2022. Available from: http://ir.bdu.edu.et/handle/123456789/14381
21. Ermyas A, Debasu. DEVELOPING AN AUTOMATIC ETHIOPIAN TEFF IDENTIFICATION SYSTEM USING MACHINE LEARNING APPROACH [Internet]. 2020. Available from: http://ir.bdu.edu.et/handle/123456789/12724
22. Wang Q, Yuan Y. Learning to resize image. Neurocomputing [Internet]. 2013 Dec 11;131:357–67. Available from: https://doi.org/10.1016/j.neucom.2013.10.007
23. Danon D, Arar M, Cohen-Or D, Shamir A. Image resizing by reconstruction from deep features. Computational Visual Media [Internet]. 2021 Apr 27;7(4):453–66. Available from: https://doi.org/10.1007/s41095-021-0216-x
24. Abdelatif MH, Madani GA, Al-Arbash AK, Oshah AA. Making noise reduction in medical imaging more accessible: machine learning and traditional techniques. Journal of Technology Research [Internet]. 2024 Dec 15;2(2):75–80. Available from: https://doi.org/10.26629/jtr.2024.10
25. Ayubi J, Amirani MC, Valizadeh M. A new content-aware image resizing based on Rényi entropy and deep learning. Neural Computing and Applications [Internet]. 2024 Mar 30;36(15):8885–99. Available from: https://doi.org/10.1007/s00521-024-09517-0
26. Aijaz O, Ali SM, Uyghur Y. Analysis of different algorithmic design techniques for seam carving. arXiv (Cornell University) [Internet]. 2024 Oct 28; Available from: http://arxiv.org/abs/2410.21207
27. Khudhair ZN, Khdiar AN, Abbadi NKE, Mohamed F, Saba T, Alamri FS, et al. Color to grayscale image conversion based on singular value decomposition. IEEE Access [Internet]. 2023 Jan 1;11:54629–38. Available from: https://doi.org/10.1109/access.2023.3279734
28. Bataineh B. Brightness and contrast enhancement method for color images via pairing adaptive gamma correction and histogram equalization. International Journal of Advanced Computer Science and Applications [Internet]. 2023 Jan 1;14(3). Available from: https://doi.org/10.14569/ijacsa.2023.0140314
29. Jing Z, Tang B. Improved image segmentation method based on Otsu thresholding and level set techniques. Journal of Physics Conference Series [Internet]. 2024 Aug 1;2813(1):012017. Available from: https://doi.org/10.1088/1742-6596/2813/1/012017
30. Sang G, Wang X, Zhang J. Improved OTSU Theory of image multi-threshold segmentation by incorporating AnT Colony Algorithm. Informatica [Internet]. 2024 Jun 4;48(9). Available from: https://doi.org/10.31449/inf.v48i9.5872
31. Soomro S, Niaz A, Soomro TA, Kim J, Manzoor A, Choi KN. Selective image segmentation driven by region, edge and saliency functions. PLoS ONE [Internet]. 2023 Dec 15;18(12):e0294789. Available from: https://doi.org/10.1371/journal.pone.0294789
32. Çağlan Ş, Değirmenci A, Çankaya İ, Göktaş ÖF. Application of watershed segmentation on biomedical images as an educational tool. Fırat Üniversitesi Mühendislik Bilimleri Dergisi [Internet]. 2025 Sep 20;37(2):763–80. Available from: https://doi.org/10.35234/fumbd.1706496
33. Bhatti MA, Syam, Chen H, Hu Y, Keung LW, Zeeshan Z, et al. Utilizing convolutional neural networks (CNN) and U-Net architecture for precise crop and weed segmentation in agricultural imagery: A deep learning approach. Big Data Research [Internet]. 2024 May 1;36:100465. Available from: https://doi.org/10.1016/j.bdr.2024.100465

34. Zhang L, Xu W, Shen C, Huang Y. Vision-Based On-Road nighttime vehicle detection and tracking using improved HOG features. Sensors [Internet]. 2024 Feb 29;24(5):1590. Available from: https://doi.org/10.3390/s24051590
35. Matuzevičius D, Urbanavičius V, Miniotas D, Mikučionis Š, Laptik R, Ušinskas A. Key-Point-Descriptor-Based image quality evaluation in photogrammetry workflows. Electronics [Internet]. 2024 May 29;13(11):2112. Available from: https://doi.org/10.3390/electronics13112112
36. Kumawat A, Panda S, Gerogiannis VC, Kanavos A, Acharya B, Manika S. A hybrid approach for image acquisition methods based on Feature-Based image registration. Journal of Imaging [Internet]. 2024 Sep 14;10(9):228. Available from: https://doi.org/10.3390/jimaging10090228
37. Li P, Fei Q, Chen Z, Liu X. Interpretable Multi-Channel Capsule Network for Human Motion Recognition. Electronics [Internet]. 2023 Oct 18;12(20):4313. Available from: https://doi.org/10.3390/electronics12204313